Effect of Phenolic Matrix Microcracking on the Structural Response of a 3-D Woven Thermal Protection System

Sarah L. Langston[1]
NASA Langley Research Center, Hampton, VA, 23681, USA

Keith H. Peterson[2]
NASA Ames Research Center, Moffett Field, CA, 94035, USA

Carl C. Poteet[3]
NASA Langley Research Center, Hampton, VA, 23681, USA

The effect of microcracking in the phenolic matrix of a three-dimensional woven thermal protection system (TPS) and the resulting material stiffness reduction was studied via a comparison of finite element analysis results from a linear analysis and an iterative linear analysis. A TPS is necessary to protect space vehicles from the aerodynamic heating of planetary entry. The Heatshield for Extreme Entry Environment Technology (HEEET) project has developed a TPS for use in high heat-flux and pressure missions. The material is a dual-layer continuous dry weave, which is then infiltrated with a low-density phenolic resin matrix to form a rigid ablator. The phenolic resin matrix does not have structural load transfer requirements, and testing has shown that the phenolic resin can fully satisfy thermal requirements when the matrix contains microcracks. Due to high stresses in the through-the-thickness direction of the material, phenolic microcracks may form in the matrix material, which would result in a reduction of stiffness. An exploratory study was conducted to determine if reduction in material stiffness would change the load paths and/or decrease the structural margins. A comparison was performed between a linear finite element analysis that did not take into account phenolic microcracking and an iterative linear finite element analysis that accounted for propagation of phenolic microcracking. Four subcases using varying assumptions were analyzed and the results indicate that the assumed strength at which the phenolic microcracking propagates was the critical parameter for determining the extent of microcracking in the phenolic matrix. Phenolic microcracking does not have an adverse effect on the structural response of the test article and is not a critical failure.

I.Introduction

Delivering payloads to the surface of other planets requires spacecraft to travel through the planet's atmosphere. The extreme aerodynamic heating experienced by an object entering these atmospheres requires the use of thermal protection systems (TPS) on spacecraft to protect the payload from the resulting high temperatures. Depending on the entry environment (atmosphere density, atmosphere composition, speed of the vehicle, etc.), different types of TPS are necessary [1]. Entry into planet atmospheres with extreme environments, such as Venus or Saturn, requires an ablative TPS. Ablators are a type of semi-passive TPS that are able to withstand high heating rates. Because they absorb heat through ablation, they are a single-use TPS [1].

The Heatshield for Extreme Entry Environment Technology (HEEET) project is a multi-year endeavor to increase the technology readiness level (TRL) of a novel three-dimensional (3-D) woven TPS. The 3-D woven TPS is designed to be mission-enabling: able to withstand high heat fluxes and entry pressures such as those on Venus or Saturn missions; and able to be tailored for each mission. Currently, missions to these planets are mass-limited due to the need to use fully-dense carbon phenolic for the TPS. The 3-D woven TPS is able to withstand similar pressures and

[1] Research Aerospace Engineer, Structural Mechanics and Concepts Branch, MS 190, AIAA member.
[2] Aerospace Engineer, Thermal Protection Materials Branch, MS 234:118
[3] Research Aerospace Engineer, Structural Mechanics and Concepts Branch, MS 190

heating rates as fully dense carbon phenolic but at a potentially lower mass, opening the trade-space for missions to these planets or other missions with similar heating rate requirements. A project goal was to raise the TRL from approximately three to six, which required a subsystem test of the technology in a relevant environment. Relevant environments for TPS would include launch loads, on-orbit transit in space, and atmospheric entry. To meet the goal of TRL 6, the HEEET project designed and built a 39-inch diameter heatshield for ground testing.

II.HEEET Material

The 3-D woven TPS, henceforth referred to as HEEET, is a 3-D layer-to-layer woven composite material. HEEET has a dual-layer architecture consisting of an outer recession layer and an inner insulating layer. The recession layer is comprised of densely woven carbon fibers. The function of the recession layer is to ablate and manage ablation during planetary entry. The insulating layer is a lower-density weave of blended carbon and phenolic yarn. The function of the insulation layer is to maintain the internal temperature below the maximum allowable. Due to the layer-to-layer weave, there are continuously woven fibers in the through-the-thickness (TTT) direction of the material. The addition of these TTT fibers leads to an increased toughness in the TTT direction compared to ablative TPS material without continuous TTT fibers. HEEET is woven in a single piece as a conformable dry weave. The dry weave is then infiltrated with low-density phenolic resin, which forms the porous phenolic matrix of HEEET. The final material is rigid. The blended yarn, the dry weave on the loom, the conformable dry weave, and the phenolic resin-infused final HEEET are shown in Figure 1.

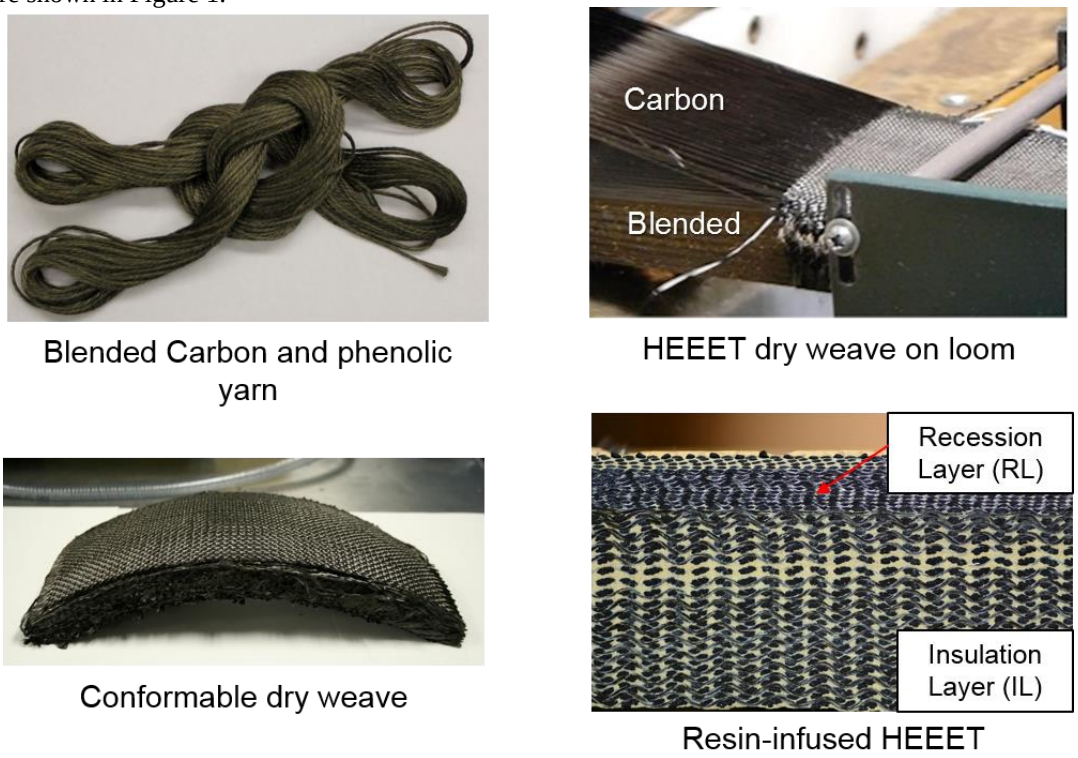

Figure 1. Clockwise from the upper left: The blended yarn constituent of the insulation layer, the HEEET dry weave on the loom, the resin-infused final HEEET material, and the conformable dry weave.

The function of the phenolic matrix is to block the flow of hot gases into the material and insulate the internal surface from excessive temperatures. There are no load transfer requirements for the matrix, as the fibers are intended to carry the mechanical load. Testing has shown that microcracked matrix material can fully satisfy the requirements to block flow and provide adequate insulation. Testing has also shown that microcracks within the phenolic are likely to form in the TTT direction under certain loading conditions. Examples of phenolic microcracking seen on a magnified image are shown in Figure 2.

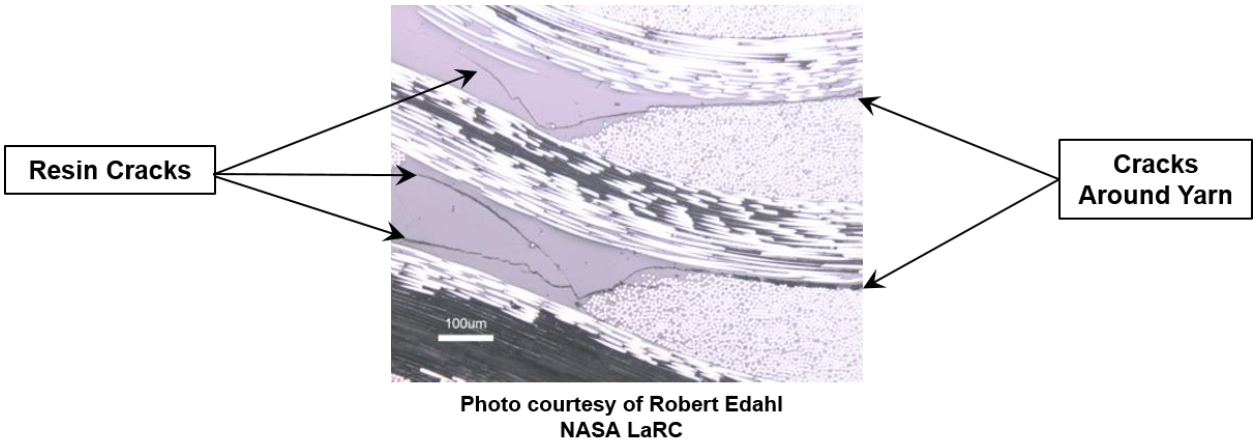

Figure 2. Polished microscopic image of the HEEET material with phenolic microcracks.

Manufacturing limitations in the width of the dry weave that can be produced drive the need for tiled heatshield architectures. In a tiled heatshield architecture, compliance is needed in the material system to reduce the bondline stresses between the tiles, thus a gap filler between the tiles is necessary. Phenolic resin cracking is used as a feature in the compliant gap filler created from HEEET to increase the compliance in the material system. Microcracked matrix in all derivatives of the HEEET material increases the compliance of the material while the fibers remain intact and provide cohesion of the material. Because microcracking does not prevent the matrix from satisfying the thermal requirement and microcracking of the matrix does not lead to critical structural failure of the material system, microcracking is not considered a material failure.

III.Engineering Test Unit

The engineering test unit (ETU) is a representative 39-inch diameter heatshield designed for a nominal Saturn mission. The test article is a 45° sphere-cone with an outer mold line shoulder radius of four inches. The heatshield is comprised of a composite carrier structure that HEEET is bonded to and an internal metallic ring for additional structural support and ground support equipment attachment. The HEEET material bonded to the exterior of the composite carrier structure consists of acreage HEEET tiles, as well as compliant gap filler and close-out plugs. The compliant gap filler and close-out plugs are created using the parent HEEET material. Further reference to HEEET in the current paper will continue to refer to the HEEET material used in the acreage tiles described in Section II. The ETU and the ETU components are shown in Figure 3.

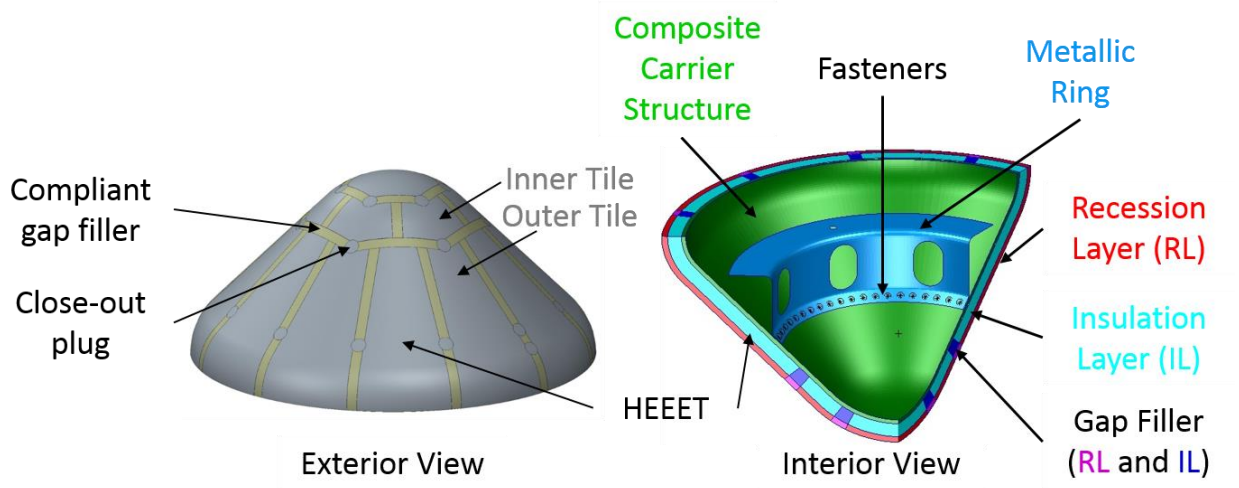

Figure 3. ETU exterior and cross-section with system components labeled.

IV.Finite Element Analysis of the ETU

While phenolic microcracking in the matrix is not considered a failure, understanding the effect of the reduction of stiffness in the material on the structural response of the system is important. Prior analysis had indicated that high stress zones within the material would produce phenolic microcracks in the TTT direction and that microcracking leads to a localized material stiffness reduction. That phenolic microcracking in the matrix would change the stress state in that localized region was known, but if the microcracks would affect the structural response of the entire ETU away from the reduced stiffness regions was unknown.

In order to preliminary investigate the effect of the localized material stiffness reduction on the entire structural response of the ETU, an exploratory study was performed. The study compared a linear finite element analysis with no material stiffness reduction taken into account with an iterative linear finite element analysis which included propagating material stiffness reduction in the insulating layer of the HEEET. The results from the exploratory study will be used to determine if the current modeling techniques are adequate to capture the structural response and also aid in the understanding of future test data.

A. Finite Element Model (FEM) of ETU

The FEM consisted of 222,476 elements (primarily solid and shell) with an approximate 0.25 inch element spacing. A convergence study was performed on the mesh to confirm that the element size was appropriate for the analysis performed. The mesh of the finite element model is shown in Figure 4.

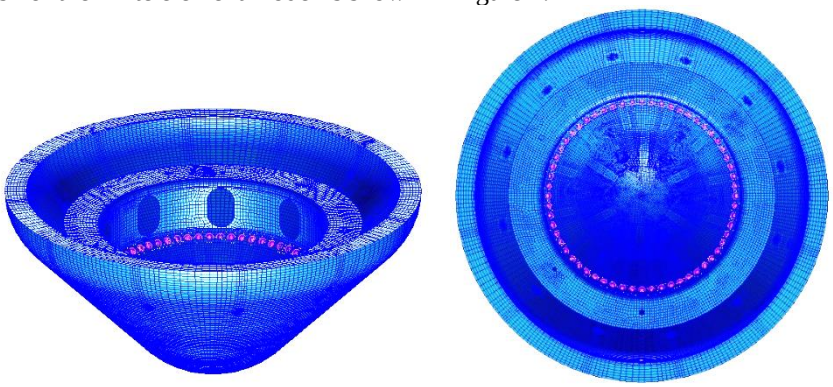

Figure 4. Isometric and interior views of the ETU finite element model mesh.

The HEEET, gap fillers, close-out plugs, and composite carrier structure were modeled with eight-node solid elements and the metallic ring was modeled with shell elements. The HEEET, gap fillers, close-out plugs, and composite carrier structure were modeled as orthotropic materials, and the metallic ring was modeled as isotropic. Previous work has shown that the cold-soak load case is the critical load case for the TTT stresses that cause phenolic microcracking. The load case consisted of an initial nodal temperature of 270 °F applied to all nodes. The initial temperature is representative of the adhesive crosslink temperature used in manufacturing and integration of the ETU. A final temperature of -250 °F was applied to all nodes. The final applied temperature was derived as the lowest operational temperature potentially seen during on-orbit transit. The initial and applied nodal temperatures result in a total applied temperature difference of -520 °F. No mechanical loads were applied. Kinematic boundary conditions were applied to eliminate rigid body motion of the model.

The fasteners between the metallic ring and the composite carrier structure were modeled using two-noded CBUSH spring-damper elements [2]. Two different approximations were applied to study the extremes of possible behavior at the bolted interface. The first approximation was derived using the Huth approximation [3], which is a semi-empirical method used to determine bolted joint stiffness. The second approximation was derived by adjusting the stiffness of the CBUSH elements to match the strain gage results from a thermal cycling test of the composite carrier structure and metallic ring prior to bonding the HEEET material on the outside of the ETU. The Huth approximation resulted

in the stiffer of the two joints. The two models will henceforth be referred to as the stiff and soft joint approximations. The effect of these two models on the extent of the phenolic microcracking was analyzed and compared.

B. Analysis Methodology for Iterative Solution of Microcrack Propagation

The macroscopic effect of phenolic microcracking can be represented as a reduction of stiffness in the material. An iterative linear analysis was performed as follows to determine the extent of the microcracking and the associated load redistribution. A linear analysis of the model was performed and any elements that exceeded a specified microcracking initiation strength in the TTT direction of the insulation layer were identified. The material properties of these elements were then replaced with a reduced stiffness material property. The load case was then re-analyzed with the updated properties. In subsequent iterations, the TTT stress in the intact elements was again compared against an initiation strength, and those that exceeded the initiation strength were assigned reduced properties. In addition, the TTT stress in the elements adjacent to a microcracked element were compared against an assumed propagation strength, which could be lower than the initiation strength. These elements were also assigned reduced properties. The pattern was repeated until the TTT stress in all elements adjacent to other microcracked elements was below the propagation strength.

The properties for the reduced stiffness HEEET insulating layer were set by reducing the TTT stiffness modulus to 1000 pounds per square inch (psi). This reduction is approximately two orders of magnitude. The in-plane and shear material moduli were reduced by the same factor. The intention of the reduction in TTT stiffness was to reduce the stiffness in the TTT direction to a negligible value while avoiding the numerical issues that would result by reducing the stiffnesses to zero.

An initiation strength of 325 psi was chosen from test data that indicated the stress at which the phenolic microcracking begins. The propagation strength was chosen as an estimate of the stress level at which the phenolic microcracking propagates in intact material that is adjacent to material with microcracks. Two different propagation strengths were studied, one where the propagation strength is equal to the initiation strength, and one where the propagation strength is much lower than the initiation strength. These two strength levels were chosen to provide estimated bounds for the exploratory study because the true propagation strength for the phenolic microcracks was unknown. A propagation strength equal to the initiation strength gathered from test data represented the upper bound of a propagation strength, and a propagation strength of 50 psi was chosen as a minimum bound in the exploratory study.

V.Results

The differences in material coefficients of thermal expansion (CTE) led to mechanical stress in the ETU when placed under only thermal loading. The large CTE mismatch between the composite carrier structure and metallic ring leads to high TTT stress in the HEEET insulating layer, specifically in the area above the ring attachment. The deformation of the ETU under the thermal load case is shown in Figure 5. The critical area for initiation of the phenolic microcracking in the HEEET insulating layer is circled in red.

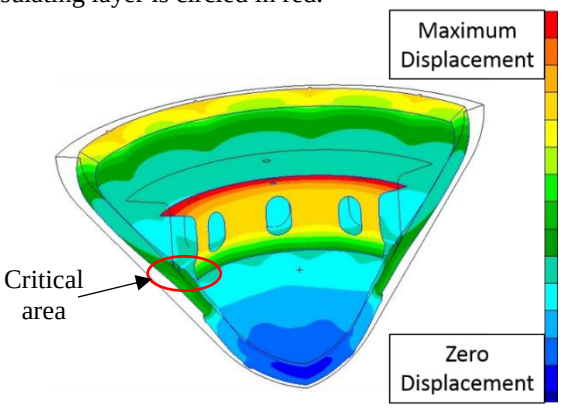

Figure 5. Cutaway view of the ETU deformation (exaggerated) under cold-soak loading. The black outline is the undeformed model and the critical area for initiation of phenolic microcracking in the insulating layer is circled in red.

The following section will present the results of the linear and iterative linear analyses for four subcases: 1) Stiff joint representation with a 325 psi propagation stress, 2) Stiff joint representation with a 50 psi propagation stress, 3) Soft joint representation with a 325 psi propagation stress, and 4) Soft joint representation with a 50 psi propagation stress. First, the total area of reduced stiffness elements will be presented along with a comparison of the final TTT stress state in the HEEET insulating layer between the linear and iterative linear analyses. Then, a discussion of the differences between the strains on the outer and inner mold lines of the vehicle will be posed. The discussion of strain results is limited to the outer mold line of the recession layer and the inner mold line of the composite carrier structure because strain gages can only be placed in these areas during testing.

A. FEM Results

Case 1: Stiff Joint; 325 psi Propagation Stress

The subcase using the stiff joint representation and 325 psi propagation stress resulted in a small area of reduced stiffness elements centered above the bolted connection on the composite carrier structure. The final reduced stiffness elements are highlighted in Figure 6. The right portion of the figure illustrates the in-plane distribution of the microcracked elements and the cut-away view highlights that the microcracking only propagated through one element through the thickness. The iterative linear solution took twenty-five iterations for the element stiffness reduction to stop propagating.

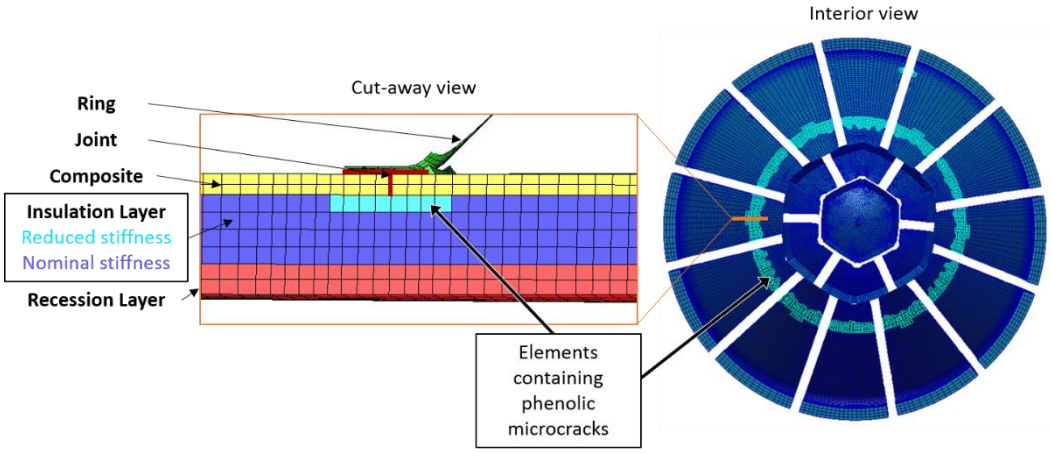

Figure 6. HEEET insulating layer with final reduced stiffness elements highlighted for the stiff joint representation at a 325 psi propagation stress. (Case 1)

The final TTT stress state in the insulation layer for both the linear and iterative linear analyses is shown in Figure 7. The linear analysis was the first analysis of the iterative linear analysis and all the elements in red in the top portion of Figure 7 represent elements that exceeded the initiation strength. The maximum stress near the ring attachment was lower in the iterative linear analysis as compared to the linear analysis that did not take into account phenolic matrix microcracking. The stress levels away from the location that experienced microcracking were unaffected by the microcracking. The ETU did not exceed material allowables in the linear analysis and remained below the material allowables throughout the iterative linear analyses. The difference in strains was also compared. Because of the experimentation limitations, only the strains on the recession layer outer mold line and composite carrier structure inner mold line were considered because those were the only viable places for strain gages to measure the strain. The strains predicted by the linear and the iterative linear analyses at the recession layer outer mold line and the composite carrier structure inner mold line (not shown) are nearly identical. Therefore, strain gage measurements cannot be used at these locations to determine which of the two analyses better represents the experimental results.

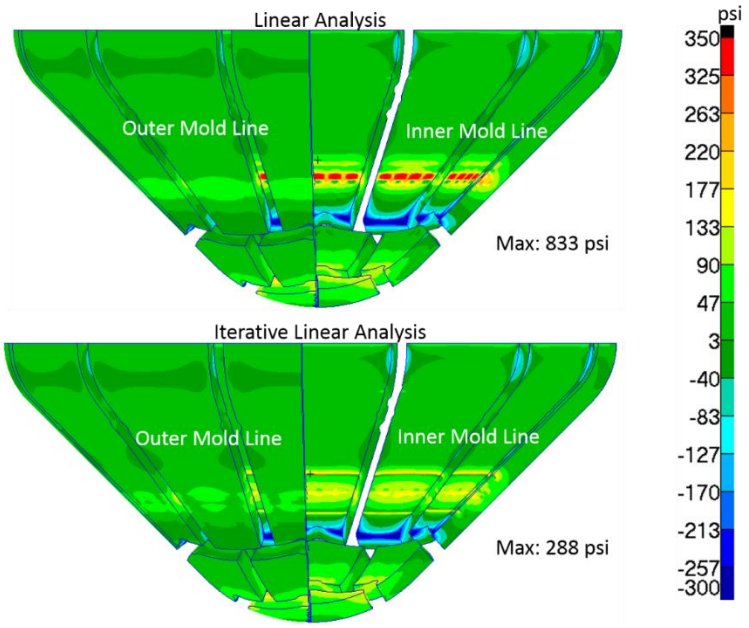

Figure 7. Comparison of TTT stress in the HEEET insulating layer for the stiff joint representation and 325 psi propagating stress. (Case 1)

Case 2: Stiff Joint; 50 psi Propagation Stress

The subcase using the stiff joint representation and 50 psi propagation stress resulted in the entire insulation layer of the outer tile [labeled in Figure 3] becoming reduced stiffness elements. The final reduced stiffness elements are highlighted in Figure 8. The tiles are fully microcracked both in-plane and through the thickness of the tile. After twenty-five iterations of the iterative linear analysis, the entire outer tile was assumed to be fully microcracked and was modeled using the reduced stiffness material property (highlighted below).

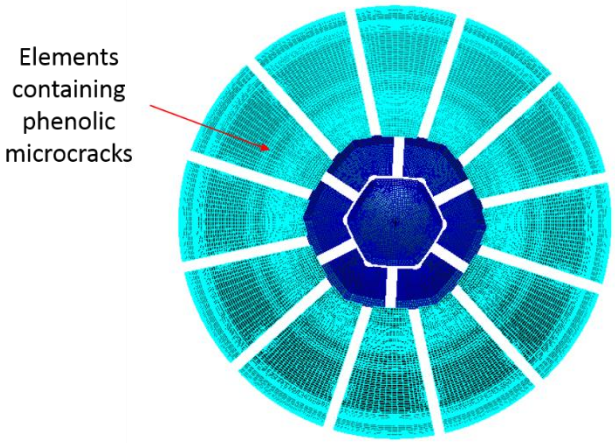

Figure 8. HEEET insulating layer with final reduced stiffness elements highlighted for the stiff joint representation with a 50 psi propagation stress. (Case 2)

The final TTT stress state in the insulation layer for both the linear and iterative linear analyses is shown in Figure 9. The linear analysis was the same as Case 1 (Figure 7) as only the propagation stress was modified and therefore the initial analysis was exactly the same FEM. The maximum stress near the ring attachment was reduced in the iterative linear analysis. However, there were some areas of increased stress in the iterative linear analysis, and there was a difference in the stress contours on the inner tiles, away from the reduced stiffness elements. In Case1, the stiff joint with a 325 psi propagation stress, there were not differences in the stress away from the microcracked elements. Additionally, there were strain differences greater than 50 microstrain at strain gage locations on the outer mold line

of the recession layer and inner mold line of the composite carrier. If the entire outer tile experiences phenolic microcracking during testing, the strain gages may be able to measure the strain. The strain gage readings would provide a possible indication that the phenolic microcracks propagated at a lower stress than the 325 psi initiation stress.

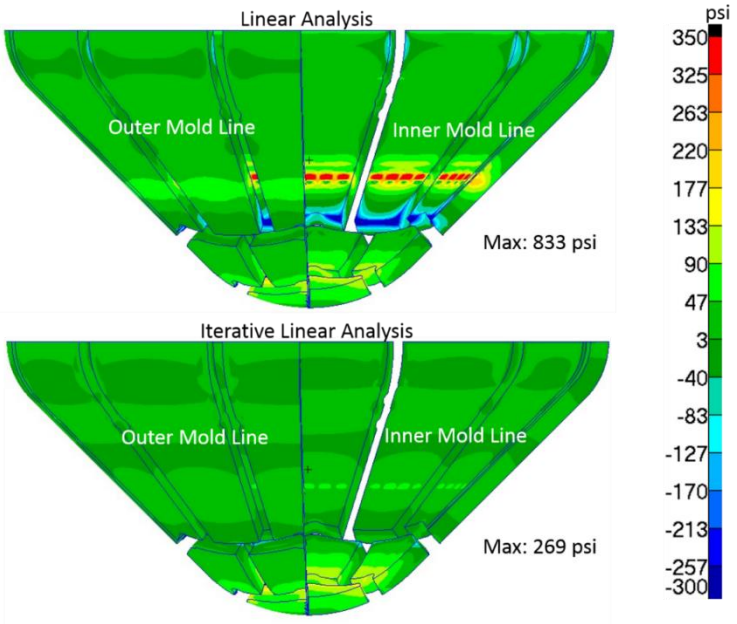

Figure 9. Comparison of TTT stress in the HEEET insulating layer for the stiff joint representation and 50 psi propagating stress. (Case 2)

Case 3: Soft Joint; 325 psi Propagation Stress

The analysis using the soft joint representation and 325 psi propagation stress resulted in a small area of reduced stiffness elements centered on the connection to the bolts, very similar to Case 1. The final reduced stiffness elements are highlighted in Figure 10. The iterative linear solution took seven iterations for the reduced stiffness elements to stop propagating.

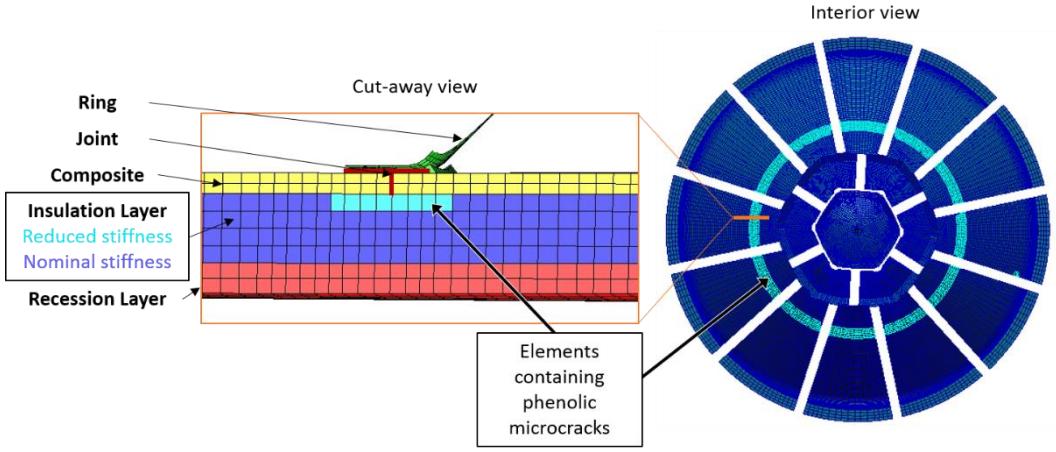

Figure 10. HEEET insulating layer with final reduced stiffness elements highlighted for the soft joint representation with a 325 psi propagation stress. (Case 3)

The final TTT stress state in the insulation layer for both the linear and iterative linear analyses is shown in Figure 11. As with the stiff joint subcases, the maximum stress was located near the ring attachment and reduced in the

iterative linear analysis. The initial linear analysis had lower final stress state than the initial linear analysis of the stiff joint. However, the final iterative linear analysis was in line with the results of the stiff joint with 50 psi propagation stress. The difference in strains on the recession layer outer mold line and composite carrier structure inner mold line were negligible between the linear and iterative linear analysis. Similar to Case 1, the differences in strain were within the noise levels of what was able to be measured via strain gages.

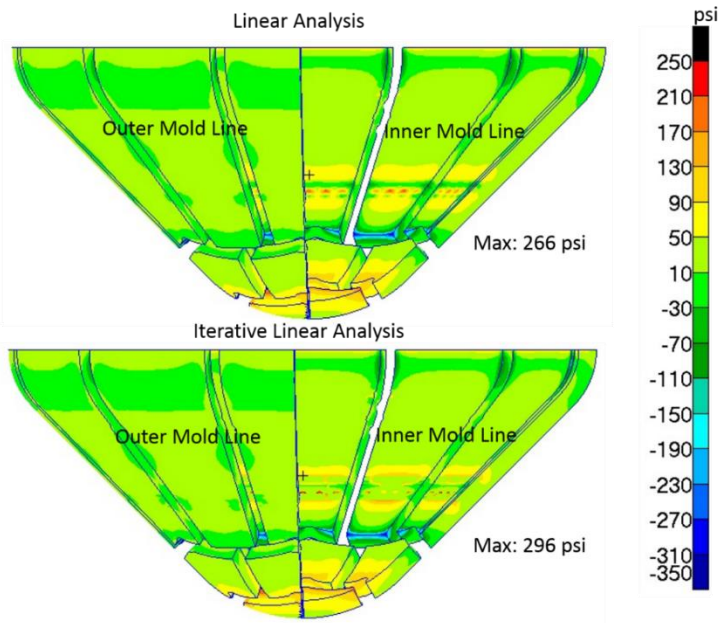

Figure 11. Comparison of TTT stress in the HEEET insulating layer for the soft joint representation and 325 psi propagating stress. (Case 3)

Case 4: Soft Joint; 50 psi Propagation Stress

The subcase using the soft joint representation and 50 psi propagation stress resulted the entire outer tile becoming reduced stiffness elements. The reduced stiffness area was the same result as the stiff joint representation and 50 psi propagation stress. The final reduced stiffness elements are highlighted in Figure 12. After twenty iterations of the iterative linear analysis, the entire outer tile was assumed to become reduced stiffness elements.

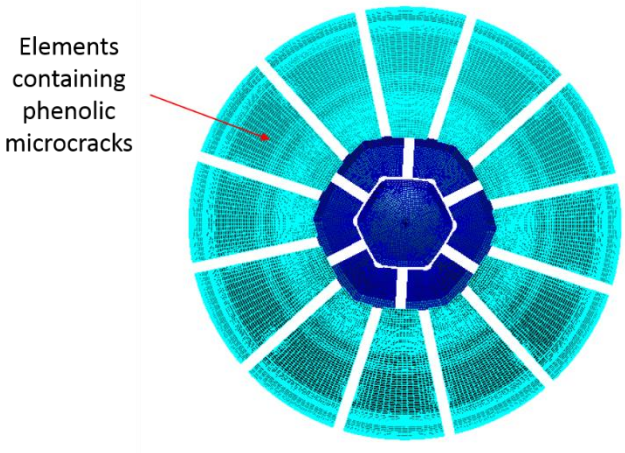

Figure 12. HEEET insulating layer with final reduced stiffness elements highlighted for the soft joint representation with a 50 psi propagation stress. (Case 4)

The final TTT stress state in the insulation layer for both the linear and iterative linear analyses is shown in Figure 13. The maximum stress was increased for the iterative linear analysis, but is reduced at the section near the bolt

attachment. There were also differences in the stress contours on the inner tiles away from the reduced stiffness elements. The strain differences were greater than 50 microstrain at strain gage locations on the outer mold line of the recession layer and inner mold line of the composite carrier. If the entire outer tile experiences phenolic microcracking during the test, the strain gage measurements should give an indication as to which analysis is more accurate.

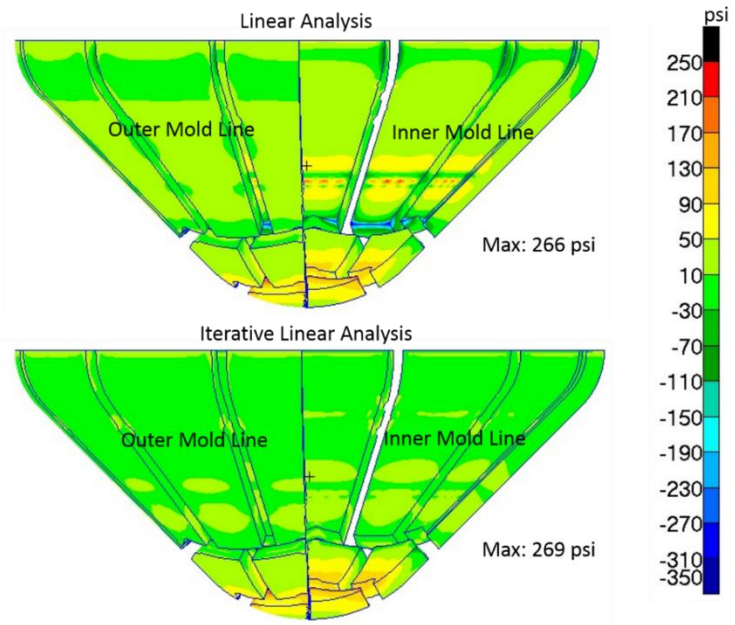

Figure 13. Comparison of TTT stress in the HEEET insulating layer for the soft joint representation and 50 psi propagating stress. (Case 4)

VI.Discussion of Results

The results of the four analysis cases indicate that the predicted final stress state is more dependent on the propagation strength of the microcracking than the joint representation. When the propagation stress was assumed to be equal to the initiation stress (325 psi), the reduction in material stiffness remained localized. When the propagation stress was assumed to be 50 psi, the phenolic microcracking and resulting reduction in material stiffness extended throughout the entire insulation layer of the outer tile. The stiff versus soft joint representations only affected in the initial area of elements that exceeded the initiation stress threshold. However, if the joint behaves similarly to the soft joint representation during the test, and the full temperature range was not met, no elements would exceed the 325 psi initiation stress and no phenolic microcracking would occur.

The reduction in material stiffness did not negatively affect any critical material allowables as compared to the linear analysis which did not take into account any phenolic microcracking. An interesting result of the study was that the phenolic microcracking and resulting material stiffness reduction did not propagate beyond the HEEET-derived gap fillers. This observation points towards the potential use of the gap filler as a crack arrestor in future designs. Of importance to note, the large TTT stress in the insulating layer above the ring was caused only by the CTE mismatch between the materials, which could be eliminated by using a different design, such as a composite ring with a CTE that is more similar to that of the HEEET and composite carrier structure.

VII.Concluding Remarks

The effect of phenolic microcracking in the HEEET insulating layer and the resulting stress distribution with reduced stiffness elements was studied via a comparison of finite element analysis results based on a linear analysis and an iterative linear analysis. Phenolic microcracking in the insulating layer has been designated as a non-critical failure by the HEEET project, and matrix with microcracks can fully satisfy the thermal requirements. The exploratory

study presented confirmed that taking into account the potential load redistribution that results from microcracking does not result in structural failure of the ETU under thermal loading.

Four different subcases were compared: a stiff joint representation with a 325 psi propagation strength, a stiff joint representation with a 50 psi propagation strength, a soft joint representation with a 325 psi propagation strength, and a soft joint representation with a 50 psi propagation strength. The results were heavily dependent on the propagation strength. A propagation strength of 325 psi (which matched the initiation strength) resulted in a localized area of reduced material stiffness centered on the ring attachment. A propagation strength of 50 psi resulted in microcracking around the entire outer tile of the heatshield. The effect of the soft and stiff joint representations was minor, as the joint stiffness affected only the results of the first cycle of the iterative analysis and not the final distribution of microcracking.

A noteworthy outcome of the exploratory study was that the phenolic microcracking never propagated beyond the HEEET-derived gap filler. The lack of microcracking beyond the gap filler points toward a potential to use the gap filler in future designs as a crack arrester. In addition, the TTT stress, which caused the phenolic microcracking in the ETU design, was due to the CTE mismatch between the composite carrier structure and the metallic ring. In future designs, the thermal mismatch could be eliminated by using materials with more similar CTEs.

Future work would include analyzing strain gauge data from the ETU testing to determine if the material behaves in the manner modeled, and which subcase most closely matches the experimental results. There is also a need to better understand and characterize the propagation stress for the phenolic microcracking, as the propagation stress was found to be a critical parameter to determine the extent of the material stiffness reduction. Determination of the propagation stress in the HEEET material could be accomplished with a test similar to a mode I fracture test.

Acknowledgements

The authors would like to thank and acknowledge the rest of the HEEET team for their work and support of the presented work. The authors would also like to thank the Game Changing Development Program and Science Mission Directorate for their funding of the HEEET project.

References

[1] Blosser, M. L., "Advanced Metallic Thermal Protection Systems for Reusable Launch Vehicles," University of Virginia, Charlottesville, VA, 2000.

[2] Anon, NSC Nastran 2012.2 Quick Reference Guide, Santa Ana, CA: MSC Software Corporation, 2012.

[3] Huth, H., "Influence of Fastener Flexibility on the Prediction of Load Transfer and Fatigue Life for Multiple-Row Joints," *Fatigue in Mechanically Fastened Composite and Metallic Joints*, West Conshohocken, PA, ASTM International, 1986, pp. 221-230.